Dual-Branch Hidden Markov Model for Rolling Bearing Degradation Analysis

Indrawata Wardhana[1,2(✉)], Amal Gouiaa-Mtibaa[3], Pascal Vrignat[3], and Frédéric Kratz[1]

[1] INSA Centre Val de Loire, PRISME Laboratory, 18000 Bourges, France
Indrawata.wardhana@insa-cvl.fr
[2] UIN Sulthan Thaha Saifuddin Jambi, 36361 Muaro Jambi, Indonesia
[3] Orléans University, PRISME Laboratory, 45000 Orléans, France

Abstract. Accurate identification of bearing faults remains a challenging task in rotating machinery monitoring due to noise contamination and pseudo-cyclostationary behavior, which obscure fault-related features, particularly in early degradation stages. To address these challenges, this paper proposes a Dual-Branch Hidden Markov Model (DB-HMM) for bearing fault diagnosis and degradation analysis. The proposed framework integrates two complementary feature branches to capture both impulsive characteristics and harmonic structures associated with characteristic fault frequencies. A dual-state formulation is introduced to enable simultaneous modeling of multiple fault components, specifically Ball Pass Frequency Outer (BPFO) and Ball Pass Frequency Inner (BPFI). By combining dual-branch feature representation with probabilistic sequential modeling, the proposed method effectively captures both temporal degradation evolution and complex signal structures. Experimental results demonstrate that the DB-HMM improves fault discrimination and enables more reliable and informative identification of degradation stages under noisy and non-stationary conditions.

Keywords: Hidden Markov Models · Envelope Signal · Bearing · Degradation Estimation

1 Introduction

Reliable detection of defects in rolling bearings remains a challenging task in the monitoring of rotating machinery. In practical industrial environments, vibration signals generated by faulty bearings are often contaminated by noise, structural vibrations, and operational variations, which may obscure fault-related signatures. Undetected defects may progressively propagate and eventually lead to severe machine failures or unexpected system shutdowns. Consequently, accurate fault diagnosis and degradation monitoring are essential for predictive maintenance and system reliability [1].

When a localized defect occurs on bearing components such as the inner race, outer race, or rolling elements, repeated interactions between rolling elements and the damaged surface generate impact events during rotation. These impacts excite the resonance

© The Author(s), under exclusive license to Springer Nature Switzerland AG 2027
O. Gervasi et al. (Eds.): ICCSA 2026 Workshops, LNCS 16760, pp. 20–36, 2027.
https://doi.org/10.1007/978-3-032-30521-3_2

modes of the surrounding mechanical structure and produce vibration signals containing useful diagnostic information about the fault. Due to the periodic motion of rolling elements relative to the defect location, the resulting vibration signals often exhibit cyclostationary characteristics. This periodic behavior produces characteristic fault frequencies (FCFs), which are commonly used as indicators for detecting and diagnosing bearing faults [2].

However, in practical operating conditions, bearing vibration signals rarely exhibit ideal cyclostationary behavior. Instead, they often demonstrate quasi-cyclostationary or pseudo-cyclostationary characteristics as shown in Fig. 1 (a). These irregularities are mainly caused by random slips between rolling elements and raceways, as well as differences in rolling speed between loaded and unloaded zones. As a result, the impact sequence generated by defective bearings may not occur in a perfectly periodic manner. This deviation from ideal cyclostationarity complicates the detection of fault-related components in the vibration signal. The problem becomes even more challenging during the early stage of degradation, where the energy of fault-related frequencies is typically very weak and can easily be masked by background noise and structural vibrations.

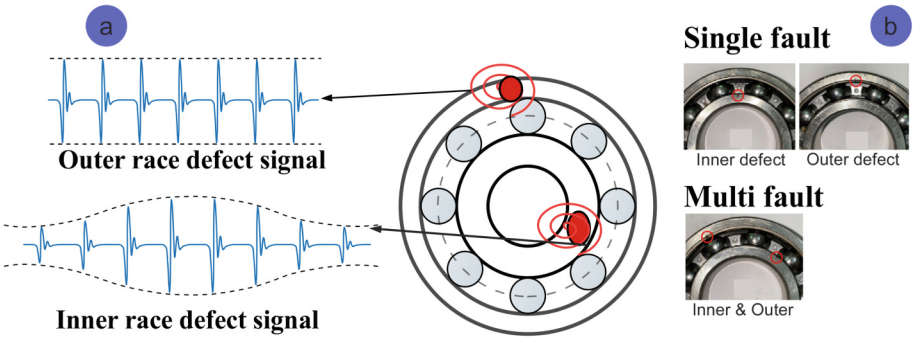

Fig. 1. (a) Pseudo-cyclostationary of bearing faults (b) Location of bearing defects [3].

In addition to pseudo-cyclostationary behavior, another difficulty arises from the complexity of fault patterns in practical bearing systems. A single localized defect usually generates periodic impacts at a specific characteristic frequency associated with the defective component. As the defect severity increases, the amplitude of the vibration response also increases. However, in many practical cases, bearings may experience multi-point defects or distributed damage on the raceway surface as illustrated in Fig. 1 (b). Such conditions can produce overlapping spectral components and nonlinear vibration responses. The interaction between multiple defects may lead to complex vibration signatures that are difficult to interpret using conventional diagnostic approaches.

Despite these challenges, characteristic fault frequencies remain an important indicator for bearing fault diagnosis. When defects evolve, harmonic components of the FCF gradually appear in the vibration spectrum [4]. These harmonic components reflect the repetitive interaction between rolling elements and defect locations. In the early stage of degradation, the harmonic components are typically weak and limited in number. As the defect grows, both the amplitude and the number of observable harmonics tend

to increase. Severe defects often produce strong higher-order harmonics, which indicate advanced damage conditions [5]. Therefore, the harmonic structure associated with FCFs can provide valuable information about the progression of bearing degradation.

Many existing approaches attempt to quantify bearing degradation using a Health index (HI) [6]. A HI is usually constructed from vibration features and is designed to represent the overall condition of the bearing. While HI-based approaches can provide a general indication of system deterioration, they often lack the ability to identify the specific location of the defect within the bearing components [7]. In other words, the health index may indicate that degradation is occurring, but it does not explicitly distinguish whether the fault originates from the inner race, outer race, or rolling elements [8]. Furthermore, many HI-based degradation models assume a monotonic degradation trend, where the health indicator gradually decreases from a healthy state toward failure [9]. In real industrial environments, however, degradation processes may not follow such an ideal monotonic behavior due to noise, load variations, and operational uncertainties.

To improve fault detection performance, various signal processing and machine learning methods have been proposed for bearing fault diagnosis [10, 11]. Traditional signal processing techniques include envelope analysis, spectral kurtosis, and time–frequency analysis, which aim to enhance impulsive components generated by localized defects. More recently, machine learning approaches such as support vector machines [12], neural networks [13], and deep learning models [14] have been applied to classify bearing fault conditions. Although these approaches can achieve high classification accuracy, many of them require large labeled datasets and may not explicitly model the temporal evolution of degradation processes.

Sequential probabilistic models provide an effective framework for analyzing time-dependent degradation processes. Among these methods, Hidden Markov Models (HMMs) are particularly suitable for modeling systems whose underlying states cannot be directly observed but can be inferred from measurable signals. In the context of bearing diagnostics, the hidden states can represent different degradation stages, while the observed vibration features provide indirect evidence of these states. Through probabilistic state transitions, HMMs can effectively capture the temporal evolution of degradation processes without relying on strictly monotonic HI.

However, conventional HMM-based approaches often rely on a single feature representation extracted from vibration signals [15]. In practice, bearing faults manifest through multiple signal characteristics, including impulsive responses, harmonic structures related to FCFs, and energy variations in specific frequency bands [16]. Relying on a single feature representation may therefore limit the ability of the model to capture the complex dynamics of bearing vibration signals, particularly under pseudo-cyclostationary conditions and noisy environments.

To address these limitations, this study proposes a DB-HMM framework for bearing fault diagnosis and degradation analysis. The proposed method integrates two complementary feature branches that capture impulsive behavior and harmonic characteristics associated with fault characteristic frequencies. In this work, the analysis focuses primarily on BPFO and BPFI components, whose spectral peaks are generally clearer and more reliable for degradation monitoring compared to Ball Spin Frequency, which

often exhibits weaker and less stable spectral signatures. By combining dual-branch feature representations with a probabilistic sequential modeling framework, the proposed method can capture both the temporal evolution of degradation and the complex structure of vibration signals.

The main contributions of this work are summarized as follows:

First, a novel DB-HMM framework is proposed to model the degradation process of rolling bearings using dual-branch feature representations.
Second, the proposed approach leverages harmonic characteristics of BPFO and BPFI components to represent the evolution of bearing degradation stages.
Third, the framework enhances robustness against pseudo-cyclostationary behavior, noise interference, and complex fault interactions.
Finally, experimental results demonstrate that the proposed method achieves improved performance for bearing fault diagnosis and degradation stage identification.

The remainder of this paper is organized as follows. Section 2 introduces the characteristics of bearing vibration signals and the background of pseudo-cyclostationary behavior. Section 3 presents the proposed DB-HMM framework and the feature extraction methodology. Section 4 describes the experimental setup and datasets used for validation. Section 5 presents the experimental results and discusses the performance of the proposed method. Finally, Sect. 6 concludes the paper and outlines directions for future work.

2 Methodology

The overall framework of the proposed DB-HMM is illustrated in Fig. 2. The method integrates two features of extraction branches, namely the envelope-based branch and the harmonic-based branch, which are combined through probabilistic modeling using HMM.

A synthetic vibration dataset is generated to simulate bearing degradation under controlled conditions, including both single-fault and multi-fault scenarios. The simulation equations are derived from industry-representative bearing vibration models and operational characteristics to ensure realistic degradation behavior. This approach enables flexible generation of both single-fault and multiple-fault degradation patterns in the desired format, without relying on publicly available benchmark datasets such as the Case Western Reserve University or Intelligent Maintenance Systems Center datasets. The main parameters used for signal generation, including system configuration and bearing geometry, are summarized in Table 1 [17].

Two degradation scenarios are considered: single-fault and multi-fault conditions. For single-fault scenarios, 20 samples are generated for each degradation state. For multi-fault scenarios, 20 samples are generated for each fault combination.

Single fault:

- BPFO degradation,
- BPFI degradation.

Multi fault:

Table 1. System configuration and bearing parameters

Parameter	Value	Parameter	Value
Sampling frequency F_S	25600 Hz	Number of balls n	8
Signal duration T	1s	Ball diameter d	7.94
Number of samples N	$F_S \bullet T$	Pitch diameter D	34.55
Rotational speed	2000 RPM	Contact angle θ	0
Rotational frequency f_S	RPM /60	Noise level σ	0.3

- BPFO: Severe, BPFI: Early,
- BPFO: Medium, BPFI: Failure,
- BPFO: Failure, BPFI: Medium.

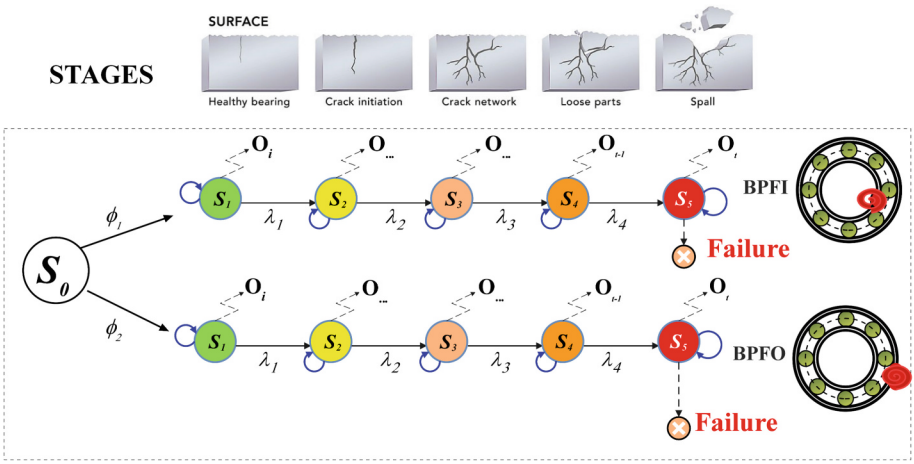

Fig. 2. Dual Branch HMM method

2.1 Bearing Fault Signal Modeling

The vibration signal of a rolling bearing is modeled as [17]:

$$x(t) = b(t) + r(t) + h(t) + n(t) \tag{1}$$

where $b(t)$ is the periodic fault impulse, $r(t)$ represents random impulses, $h(t)$ denotes harmonic components, and $n(t) \sim \mathcal{N}(0, \sigma^2)$ is additive Gaussian noise.

2.2 Fault Impulse Modeling

The fault-induced impulsive component is defined as:

$$b(t) = \sum_i A \cdot e^{-\beta_1 * \left(t - \frac{i}{f_m}\right)} \cdot sin\left(2\pi f_r \left(t - \frac{i}{f_m}\right)\right) \tag{2}$$

Two fault types are considered: Outer race fault $A_i \sim \mathcal{U}(0.9,1)$ and Inner race fault $A_i = \frac{1-sin(2\pi f_r t)}{2}$, where f_m is the fault characteristic frequency and f_r is the rotational frequency.

2.3 Harmonic Components

The harmonic component is defined as:

$$h(t) = \sum_{k=1}^{K} Psin(2\pi h_k t + \theta_k) \tag{3}$$

2.4 Envelope Signal and Generalized Envelope Spectrum

The analytic signal is defined using the Hilbert transform:

$$\alpha(t) = x(t) + j\mathcal{H}(x(t)) \tag{4}$$

where $\mathcal{H}$ denotes the Hilbert transform. The conventional envelope signal is:

$$E(t) = |\alpha(t)| = \sqrt{x^2(t) + \mathcal{H}^2\{x(t)\}} \tag{5}$$

The generalized envelope is defined using a parameter υ [18]:

$$GE_\upsilon(t) = \begin{cases} log(\lceil \alpha(t) \rceil), & \upsilon = 0 \\ \lceil \alpha(t) \rceil^\upsilon, & \upsilon > 0 \end{cases} \tag{6}$$

The corresponding Generalized Envelope Spectrum (GES) is obtained via Fourier transform:

$$GES_\upsilon(f) = \mathcal{F}\{GE_\upsilon(t)\} \tag{7}$$

where $\mathcal{F}(\cdot)$ denotes the Fourier transform. The parameter ν controls feature enhancement, where $\nu > 1$ improves robustness to noise, while $\nu < 1$ enhances impulsive components.

2.5 Feature Extraction

The degradation characteristics are represented using logarithmic and ratio-based harmonic features:

$$F_1 = log_{10}(H_1)\ F_2 = log(H_2 + H_3 + H_4) \tag{8}$$

The feature vector is given by $X = [F_1, F_2]$. For clustering, a reduced feature space is adopted $X_c = [F_1, F_5]$.

2.6 Gaussian Mixture Model

The probability density of the feature vector is modeled using a mixture of Gaussian distributions [19]:

$$p(x) = \sum_{i=1}^{k} w_i \mathcal{N}(x|\mu_i, \Sigma_i) \tag{9}$$

where w_i, μ_i, and Σ_i denote the mixture weight, mean vector, and covariance matrix of the i-th Gaussian component. Each sample is assigned to a discrete observation symbol:

$$o_t = \underset{i}{argmax} P(i|x_t) \tag{10}$$

This process converts continuous features into discrete states suitable for HMM modeling. The observation sequence is defined as:

$$o = \{o_1, o_2, \ldots, o_T\} \tag{11}$$

2.7 Dual-Branch Hidden Markov Model

To model the temporal evolution of bearing degradation, a HMM is employed. The HMM is defined by three parameters [20]:

$$\lambda = (A, B, \pi) \tag{12}$$

where A: state transition probability matrix, B: observation probability matrix, π: initial state distribution

State Definition

$$s_1, s_2, s_3, s_4, s_5 = \{Healthy, Early, Medium, Severe, Failure\} \tag{13}$$

These states model the progressive evolution of bearing damage from a healthy condition to failure. For two Branch states are defined as:

$$s_t = \left(s_t^{(1)}, s_t^{(2)}\right) \tag{14}$$

where $s_t^{(1)}$ and $s_t^{(2)}$ represent the degradation states of Branch 1 and Branch 2, respectively.

State Transition Model

The transition probability matrix is defined as:

$$\mathcal{P}(s_{t+1}|s_t) = \mathcal{P}\left(s_{t+1}^{(1)}\middle|s_t^{(1)}\right) \cdot \mathcal{P}\left(s_{t+1}^{(2)}\middle|s_t^{(2)}\right) \tag{15}$$

Each transition matrix follows a left-to-right structure:

$$a_{ij}^{(k)} = 0 \, for \, j < i, k \in \{1,2\} \tag{16}$$

This constraint ensures that the degradation process is irreversible.

Dual-Branch Observation Modeling

Unlike conventional HMM approaches that rely on a single feature representation, the proposed method employs two complementary observation Branches: Branch 1 (BPFO) and Branch 2 (BPFI). Each Branch generates an observation sequence:

$$o^{(1)} = \left\{o_1^{(1)}, \ldots, o_T^{(1)}\right\}, o^{(2)} = \left\{o_1^{(2)}, \ldots, o_T^{(2)}\right\} \tag{17}$$

The observation probability for each state is modeled as the joint likelihood of both Branches:

$$P(o_t|s_t) = P\left(o_t^{(1)}|s_t\right) \cdot P\left(o_t^{(2)}|s_t\right) \tag{18}$$

This formulation assumes conditional independence between the two branches while enabling probabilistic fusion of complementary information. Although both branches are derived from the same vibration signal. After conditioning on the hidden health state, both branches are assumed to provide complementary diagnostic information with reduced dependency.

From a signal-processing perspective, vibration signals contain multiple overlapping fault components in both temporal and frequency domains. The separation of BPFO and BPFI components through dedicated feature extraction reduces the correlation between observation branches and supports effective probabilistic fusion. Therefore, the conditional independence assumption is adopted as a practical simplification for the proposed HMM framework.

Observation Probability Matrix.

For each branch, the observation probability matrix is defined as:

$$B^{(k)} = \left[b_j^{(k)}(m)\right], b_j^{(k)}(m) = P\left(o_t^{(k)} = m|s_t = j\right) \tag{19}$$

where $k \in \{1,2\}$ denotes the Branch index and m represents the discrete observation symbol obtained from GMM clustering. The final observation likelihood is obtained by combining both matrices:

$$b_j(m) = b_j^{(1)}(m) \cdot b_j^{(2)}(m) \tag{20}$$

Initial State Distribution and Prior Modeling

The initial state distribution is defined as:

$$\pi = \pi^{(1)} \cdot \pi^{(2)} \tag{21}$$

For the dual-branch formulation, the prior probability of observations is expressed as:

$$\pi^{(1)} = [1,0,\ 0,0,\ 0],\ \pi^{(2)} = [1,0,\ 0,0,\ 0] \tag{22}$$

This reflects the parallel contribution of both feature branches at the initial stage.

State Inference

Given the trained model, the most probable hidden state sequence is obtained using the Viterbi algorithm:

$$s^* = \underset{s}{argmax} P(s|o, \lambda) \tag{23}$$

where $s = \{s_1, s_2, \ldots, s_T\}$ represents the hidden degradation states. This enables tracking of degradation progression over time.

Interpretation

This formulation allows simultaneous tracking of degradation states, for example:

$$(Normal, Normal) \rightarrow (Medium, Early) \rightarrow (Failure, Medium) \tag{24}$$

3 Results and Discussion

This section presents a comprehensive evaluation of the proposed Dual-Branch Hidden Markov Model (DB-HMM) for bearing degradation analysis. The analysis is conducted from multiple perspectives, including time-domain signal characteristics, spectral behavior, feature representation, multi-fault tracking capability, transition dynamics, and classification performance.

3.1 Time-Domain Signal Characteristics

The time-domain vibration signals provide direct insight into the evolution of fault-induced impulses. Figure 3 shows the BPFO signals under different degradation stages. In the early stage, the signal exhibits weak and sparse impulsive components, which are often masked by noise. As degradation progresses, the impulses become more frequent and exhibit higher amplitudes, indicating stronger interactions between rolling elements and defect surfaces. In the severe and failure stages, impulsive behavior becomes highly periodic and dominant, reflecting significant structural damage.

In contrast, Fig. 4 presents the vibration signals for BPFI. Due to the rotating nature of inner race defects, the signal exhibits amplitude modulation effects, resulting in more irregular and less stable patterns. This behavior makes early fault detection more challenging compared to BPFO.

Figure 5 illustrates vibration signals under combined fault conditions. In the first case (Fig. 5 (a)), the signal is dominated by strong and highly periodic impulsive components. This behavior is mainly associated with the severe BPFO fault, which produces consistent high amplitude impacts due to repeated interactions between rolling elements and the outer race defect. The presence of the BPFI medium fault introduces additional modulation, although its contribution is less dominant.

In contrast, the second case (Fig. 5 (b)) exhibits more irregular and fluctuating impulsive patterns. The BPFI failure condition introduces strong amplitude modulation due to the rotating nature of the inner race defect, resulting in a less stable signal structure. Meanwhile, the BPFO medium fault contributes to weaker and less consistent impacts. These results highlight that different fault components contribute differently to the overall vibration signal depending on their severity levels. Outer race defects tend to produce

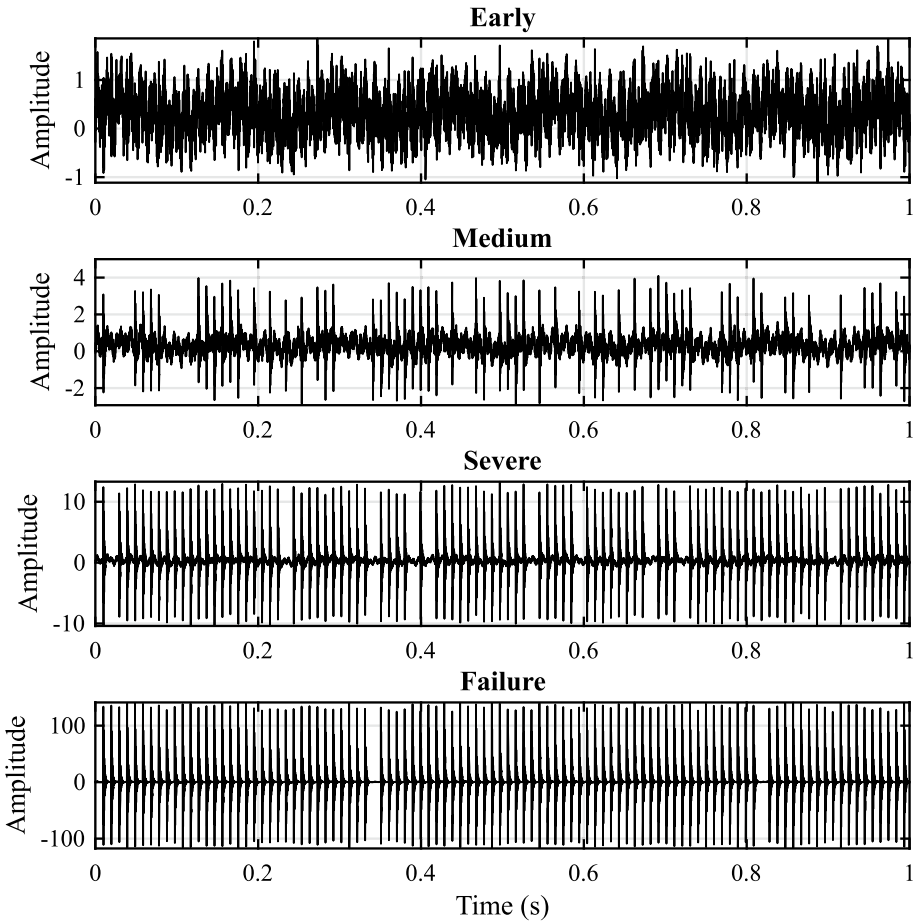

Fig. 3. Time-domain vibration signals under different fault severity levels (Early–Failure) for BPFO

more stable and periodic impulsive signatures, whereas inner race defects generate more complex and modulated patterns. This difference confirms the necessity of a dual-branch modeling approach. By separating the contributions of different fault components, the proposed DB-HMM can better capture heterogeneous degradation behaviors that cannot be represented using a single-state model.

To enhance fault-related features, the GES is applied. Figure 6 shows that the harmonic structure associated with BPFO becomes increasingly pronounced as degradation progresses. In the early stage, only low-order harmonics were visible with weak amplitudes. As the fault evolves, higher-order harmonics emerge and their amplitudes increase significantly, indicating stronger periodic impacts.

For BPFI Fig. 7, the harmonic structure is less stable due to pseudo-cyclostationary behavior caused by varying contact conditions. Despite this complexity, GES remains

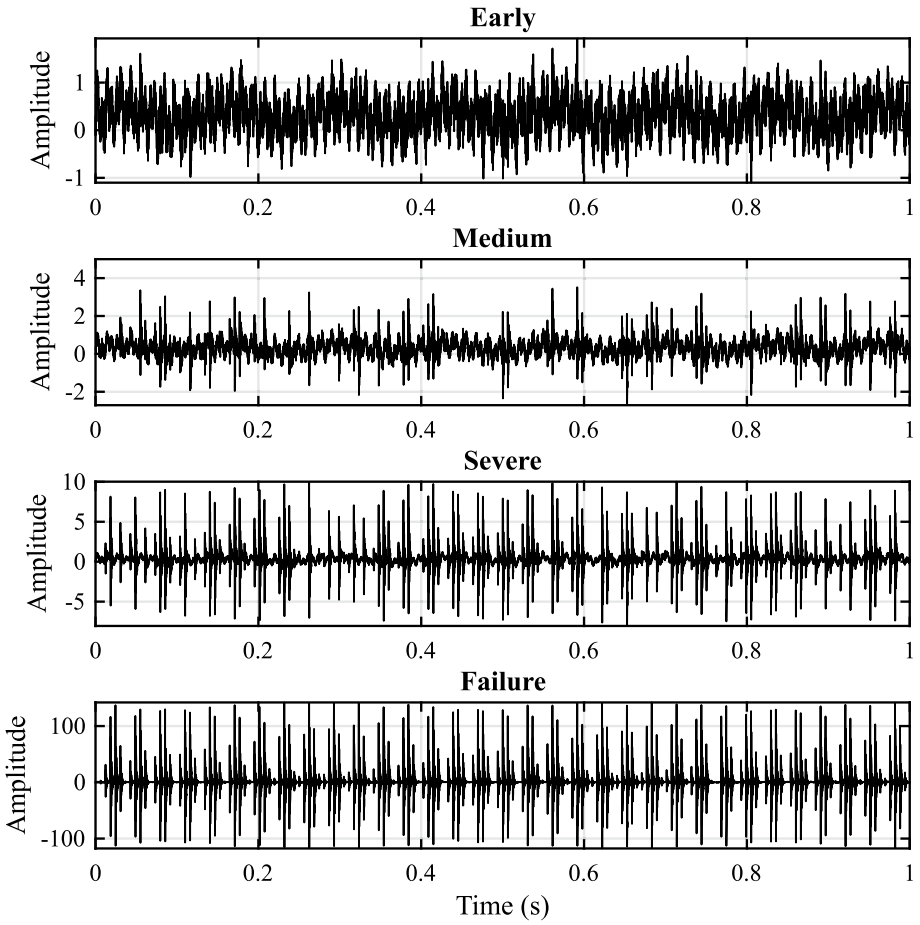

Fig. 4. Time-domain vibration signals under different fault severity levels (Early–Failure) for BPFI.

effective in highlighting fault-related components, demonstrating its robustness under non-ideal operating conditions.

The extracted harmonic features are transformed into a compact representation and clustered using a GMM, as illustrated in Fig. 8. This step converts continuous feature space into discrete observation symbols suitable for HMM modeling. As shown in Fig. 6(a), the clustering results for BPFO exhibit a clear and well-structured separation between degradation stages. The clusters are distributed along a monotonic progression, where samples corresponding to healthy conditions are concentrated in the lower feature region, while severe and failure states occupy higher feature values. The Gaussian components form compact and well-separated ellipsoidal regions, indicating low intra-cluster variance and strong discriminative capability. This behavior reflects the relatively stable and periodic impulsive characteristics of BPFO faults, which result in consistent harmonic patterns in the GES domain.

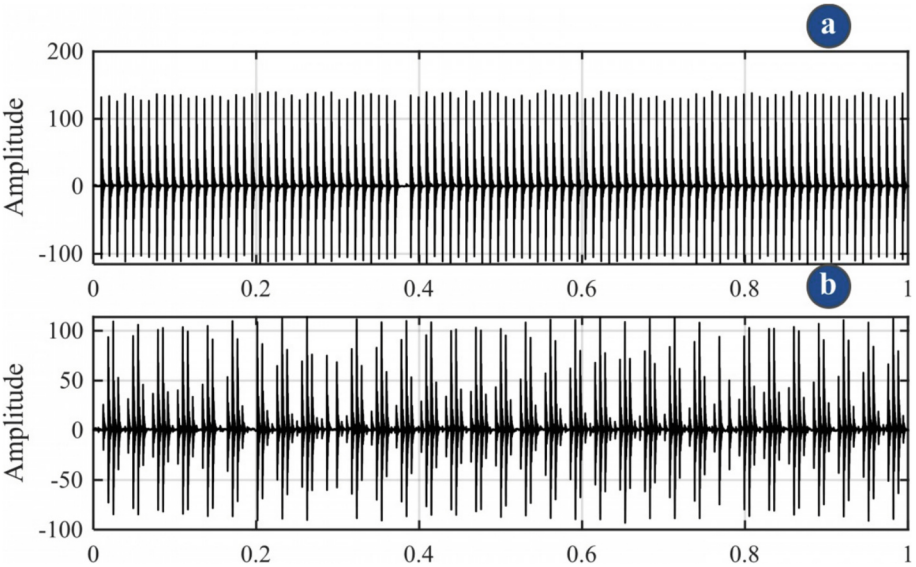

Fig. 5. Time-domain vibration signals (a) BPFO: Medium, BPFI: Failure (b) BPFO: Failure, BPFI: Medium

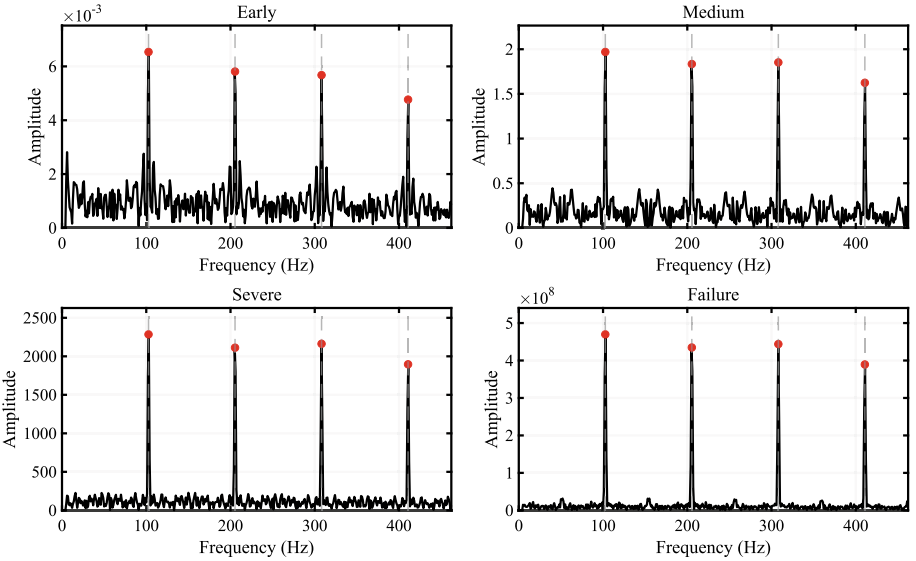

Fig. 6. GES of BPFO under different degradation stages

In contrast, Fig. 6(b) shows the clustering results for BPFI, which exhibit a more scattered and overlapping distribution. Although the overall progression from healthy to faulty states is still observable, the cluster boundaries are less distinct compared to BPFO. This behavior is attributed to the rotating nature of inner race defects, which

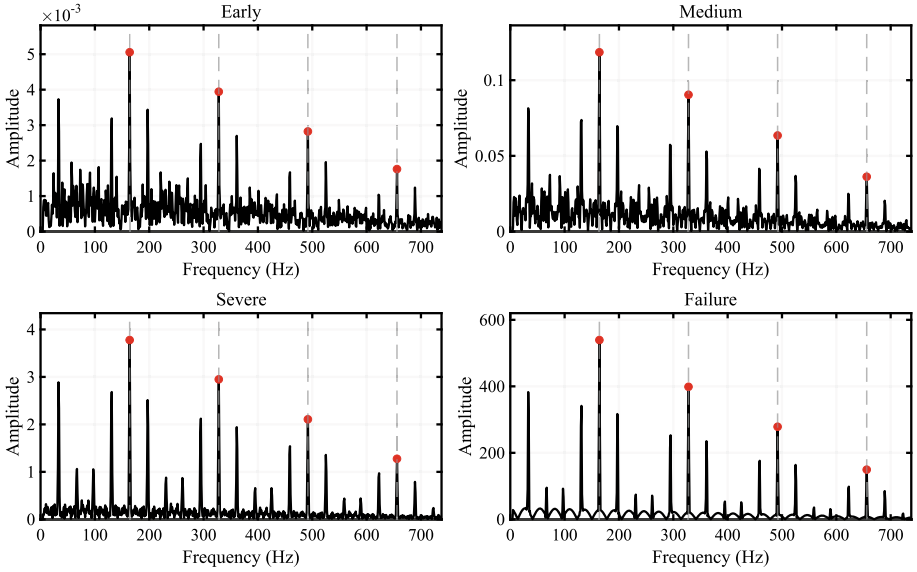

Fig. 7. GES of BPFI under different degradation stages

introduces amplitude modulation and pseudo-cyclostationary effects. As a result, the extracted features show higher variability, leading to increased overlap between adjacent degradation states.

Despite the increased variability in BPFI, the GMM is still able to capture the general trend of degradation and provide meaningful discretization. The ordering of clusters based on feature magnitude ensures a consistent mapping between observation symbols and degradation levels, which is essential for constructing reliable observation sequences in the DB-HMM framework.

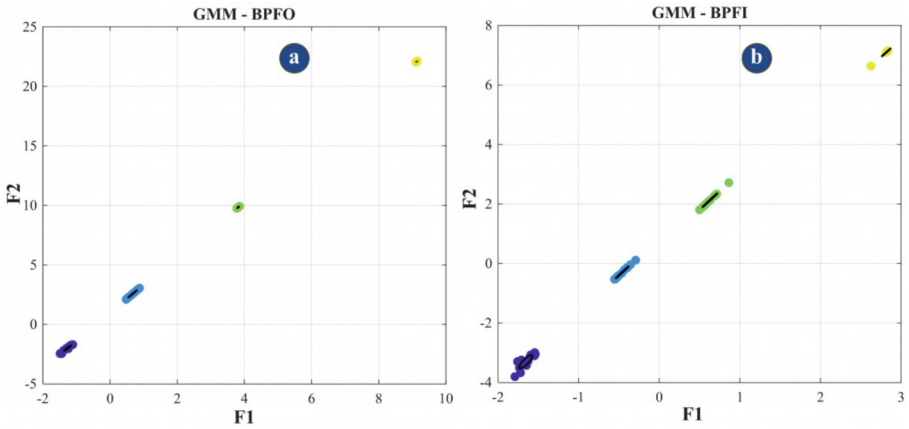

Fig. 8. GMM clustering results in the feature space: (a) BPFO and (b) BPFI.

The dataset is divided into training and testing sets using a 30:70 ratio. The training data are used to estimate the DB-HMM parameters, while the testing data are used for evaluation. The learned transition matrices provide important insight into degradation dynamics. Both matrices exhibit strong diagonal dominance, indicating that each degradation state persists over time before transitioning to the next stage. This behavior aligns with the physical nature of bearing degradation, which evolves gradually rather than abruptly. A representative transition matrix for Branch 1 and the transition matrix for Branch 2 are:

$$A^{(1)} = \begin{bmatrix} 0.992 & 0.008 & 0 & 0 & 0 \\ 0 & 0.933 & 0.067 & 0 & 0 \\ 0 & 0 & 0.929 & 0.071 & 0 \\ 0 & 0 & 0 & 0.929 & 0.071 \\ 0 & 0 & 0 & 0 & 1 \end{bmatrix}$$

$$A^{(2)} = \begin{bmatrix} 0.991 & 0.009 & 0 & 0 & 0 \\ 0 & 0.920 & 0.080 & 0 & 0 \\ 0 & 0 & 0.915 & 0.085 & 0 \\ 0 & 0 & 0 & 0.905 & 0.095 \\ 0 & 0 & 0 & 0 & 1 \end{bmatrix}$$

Furthermore, differences between $A^{(1)}$ and $A^{(2)}$ suggest that the degradation rates are not identical. Branch 2 shows higher self-transition probabilities in early states, indicating a slower and more gradual evolution compared to Branch 1. This confirms that the learned transition matrices are not arbitrary but reflect physically meaningful degradation behavior.

The classification performance is evaluated using confusion matrices, as presented in Fig. 9 for BPFO, BPFI, and multi-defect conditions. In both single-fault cases (Fig. 9 (a) and Fig. 9 (b)), the results show a perfect diagonal structure, indicating that all samples are correctly classified into their respective degradation states. This strong diagonal dominance confirms that the proposed feature representation effectively separates the degradation levels in the feature space. In particular, the distinction between Medium, Severe, and Failure states is highly consistent, reflecting the increasing strength of impulsive and harmonic components as the fault progresses.

For the multi-defect scenario (Fig. 9 (c)), the results also demonstrate accurate classification of combined fault states. The model successfully identifies different degradation levels between BPFO and BPFI simultaneously, as shown by the correct mapping of state combinations. This indicates that the proposed dual-branch framework can capture heterogeneous degradation behaviors across multiple fault components. Despite the inherent difficulty in detecting early-stage faults due to weaker signal characteristics, the proposed approach maintains high classification performance across all conditions. This highlights the benefit of combining complementary feature domains and probabilistic modeling. Overall, the results achieve an accuracy of 100% for all evaluated cases. It should be noted that the high accuracy is partly influenced by using synthetically generated data under controlled conditions, which ensures clear separation between degradation states.

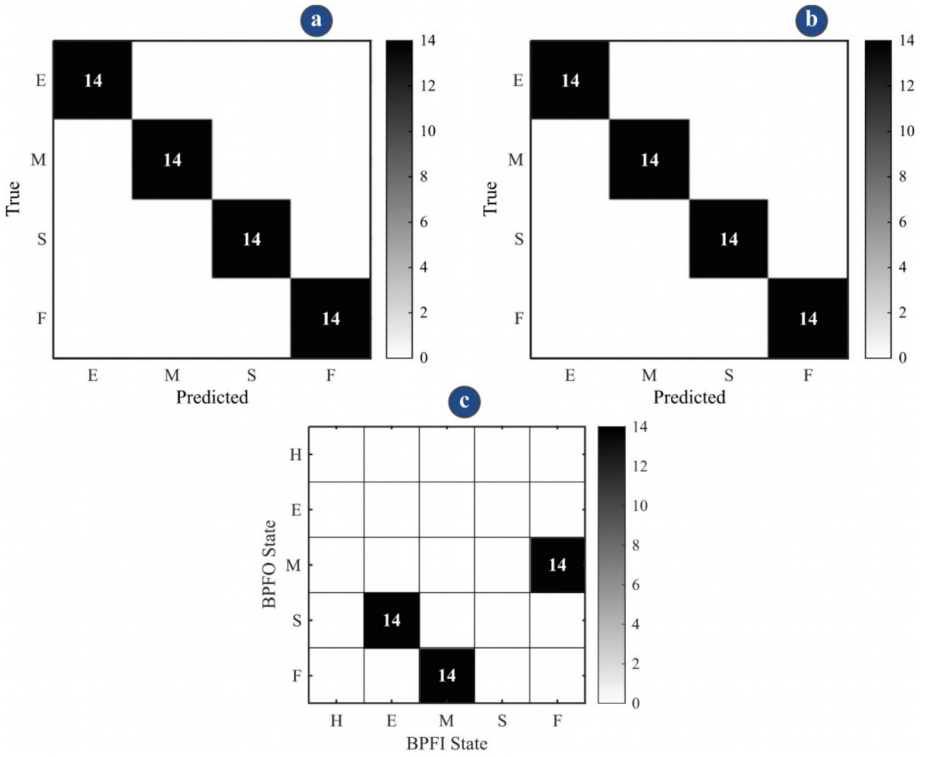

Fig. 9. Confusion matrices for bearing fault degradation classification: (a) BPFO, (b) BPFI, and (c) multi-defect BPFO–BPFI. The labels denote degradation states: Early (E), Medium (M), Severe (S), and Failure (F).

4 Conclusion

This paper proposed a DB-HMM for bearing degradation analysis. This method integrates two complementary feature branches and enables simultaneous tracking of multiple fault types through a dual-state formulation. Experimental results show that the proposed approach effectively captures degradation progression and improves fault discrimination under noisy and pseudo-cyclostationary conditions. Future work will focus on extending the framework to more complex multi-fault scenarios and real industrial applications.

References

1. Mohanty, S., Gupta, K.K., Raju, K.S.: Hurst based vibro-acoustic feature extraction of bearing using EMD and VMD. Meas. J. Int. Meas. Confed. **117**, 200–220 (2018)
2. Sacerdoti, D., Strozzi, M., Secchi, C.: A comparison of signal analysis techniques for the diagnostics of the IMS rolling element bearing dataset. Appl. Sci. Switz. **13**(10) (2023). https://doi.org/10.3390/app13105977

3. Abbasi, M.A., Huang, S., Khan, A.S.: Fault detection and classification of motor bearings under multiple operating conditions. ISA Trans. **156**, 61–69 (2025). https://doi.org/10.1016/j.isatra.2024.11.008
4. Zhou, Q., Yi, C., Yan, L., Huang, C., Lin, J.: A blind deconvolution approach based on spectral harmonics-to-noise ratio for rotating machinery condition monitoring. IEEE Trans. Autom. Sci. Eng. **20**(2), 1092–1107 (2023). https://doi.org/10.1109/TASE.2022.3179457
5. Shi, Z., Liu, J., Xiao, G.: Analysis of cage slip and impact force in a cylindrical roller bearing with race defects. Tribol. Int. **180**, 108208 (2023). https://doi.org/10.1016/j.triboint.2022.108208
6. Ren, J., Zhang, J., Wang, J., Zhao, X.: Recursive signal denoising method for predictive maintenance of equipment by using deep learning based temporal masking. Comput. Ind. Eng. **188**, 109921 (2024). https://doi.org/10.1016/j.cie.2024.109921
7. Bilendo, F., Badihi, H., Lu, N., Jiang, B.: A data-driven prognostics method for explicit health index assessment and improved remaining useful life prediction of bearings. ISA Trans. (2021). https://doi.org/10.1016/j.isatra.2021.05.007
8. Zhong, J., Wang, D., Li, C.: A nonparametric health index and its statistical threshold for machine condition monitoring. Measurement **167**, 108290 (2021). https://doi.org/10.1016/j.measurement.2020.108290
9. Avendano, D.N., Vandermoortele, N., Soete, C.: A semi-supervised approach with monotonic constraints for improved remaining useful life estimation. Sensors (2022). https://www.mdpi.com/1424-8220/22/4/1590
10. Tang, Z., Wang, M., Ouyang, T., Che, F.: A wind turbine bearing fault diagnosis method based on fused depth features in time–frequency domain. Energy Rep. **8**, 12727–12739 (2022). https://doi.org/10.1016/j.egyr.2022.09.113
11. Al Mamun, A., et al.: Multi-channel sensor fusion for real-time bearing fault diagnosis by frequency-domain multilinear principal component analysis. Int. J. Adv. Manuf. Technol. **124**(3–4), 1321–1334 (2023). https://doi.org/10.1007/s00170-022-10525-4
12. Goyal, D., Choudhary, A., Pabla, B.S., Dhami, S.S.: Support vector machines based non-contact fault diagnosis system for bearings. J. Intell. Manuf. **31**(5), 1275–1289 (2020). https://doi.org/10.1007/s10845-019-01511-x
13. Liu, Y., Wang, Y., Wang, Y., Xue, S., Wang, Z., Gao, Z.: Method for predicting remaining useful life of rolling bearings based on dynamic complexity characteristic entropy and quantum neural networks. Eng. Fail. Anal. **170**, 109315 (2025). https://doi.org/10.1016/j.engfailanal.2025.109315
14. Ayman, A., Onsy, A., Attallah, O., Brooks, H., Morsi, I.: Feature learning for bearing prognostics: a comprehensive review of machine/deep learning methods, challenges, and opportunities. Measurement 116589 (2024). https://doi.org/10.1016/j.measurement.2024.116589
15. Jiang, H., et al.: Bearing performance degradation assessment based on SC-RMI and Student's t-HMM. Materials **14**(20), 6077 (2021). https://doi.org/10.3390/ma14206077
16. Patil, A.P., Mishra, B.K., Harsha, S.P.: Fault diagnosis of rolling element bearing using autonomous harmonic product spectrum method. Proc. Inst. Mech. Eng. Part K J. Multi-Body Dyn. **235**(3), 396–411 (2021). https://doi.org/10.1177/1464419321994986
17. Cheng, H., et al.: A novel bearing fault diagnosis method based on improved product envelope spectrum Gini coefficient ratio optimization gram. Mech. Syst. Signal Process. **239**, 113349 (2025). https://doi.org/10.1016/j.ymssp.2025.113349
18. Schmidt, S., Wilke, D.N., Gryllias, K.C.: Generalised envelope spectrum-based signal-to-noise objectives: formulation, optimisation and application for gear fault detection under time-varying speed conditions. Mech. Syst. Signal Process. **224**, 111974 (2025). https://doi.org/10.1016/j.ymssp.2024.111974

19. Fu, Y., Liu, X., Sarkar, S., Wu, T.: Gaussian mixture model with feature selection: an embedded approach. Comput. Ind. Eng. **152**, 107000 (2021)
20. Wardhana, I., Gouiaa-Mtibaa, A., Vrignat, P., Kratz, F.: Contribution to estimating the level of bearing degradation using a Multi-Branch Hidden Markov Model approach. Comput. Ind. **167**, 104254 (2025). https://doi.org/10.1016/j.compind.2025.104254